Biochimica et Biophysica Acta 1837 (2014) 1643–1652

Contents lists available at ScienceDirect

Biochimica et Biophysica Acta

journal homepage: www.elsevier.com/locate/bbabio

Superoxide production by cytochrome bc_1 complex: A mathematical model

F. Guillaud [a,d], S. Dröse [b,1], A. Kowald [a], U. Brandt [b,c], E. Klipp [a,*]

[a] Theoretische Biophysik, Humboldt University, Invalidenstraße 42, 10115, Berlin, Germany
[b] Molecular Bioenergetics Group, Medical School, Goethe University, Frankfurt am Main, Germany
[c] Nijmegen Centre for Mitochondrial Disorders, Radboud University Medical Centre, Geert Grooteplein-Zuid 10, 6525GA Nijmegen, The Netherlands
[d] INSERM U1082, University of Poitiers, Faculty of Medicine and Pharmacy, CHU of Poitiers, 6 rue de la Milétrie, 86021 Poitiers, France

ARTICLE INFO

Article history:
Received 5 October 2013
Received in revised form 28 May 2014
Accepted 30 May 2014
Available online 7 June 2014

Keywords:
Mathematical model
Complex III
Reactive oxygen species
Superoxide
Antimycin A

ABSTRACT

Reactive oxygen species (ROS) are involved in the pathophysiology of several diseases (*e.g.* Alzheimer or atherosclerosis) and also in the aging process. The main source of ROS in aerobic organisms is the electron transport chain (ETC) in the inner mitochondrial membrane. Superoxide is produced at complexes I and III of the ETC, starting a complex network of ROS reactions. To achieve a deeper mechanistic understanding of how ROS are generated by complex III, we developed a mathematical model that successfully describes experimental data of complex III activity in various rat tissues, the production of ROS with and without antimycin and ROS generation depending on different values of the membrane potential $\Delta\Psi$. The model also reinforces the idea of ubiquinone acting as a redox mediator between heme b_L and oxygen, as proposed earlier.

1. Introduction

In 1956, Harman [1] proposed that reactive oxygen species (ROS) are at the center of the aging process. ROS, such as the superoxide anion ($O_2^{\cdot-}$), hydrogen peroxide (H_2O_2) or the hydroxyl radical (HO•), are highly reactive byproducts of oxygen metabolism, and are able to damage all biologically relevant molecules (proteins, lipids, DNA) of the cell. The role of ROS for the aging process has been investigated in numerous studies [2–8], but nevertheless the exact mechanisms of ROS production and the reactions involved remain poorly understood [9,10]. Furthermore, ROS are involved in many diseases and play an important role as cell signaling molecules for various processes [11].

The majority of ROS are produced by the mitochondrial electron transfer chain, more precisely by complex I (NADH:ubiquinone oxidoreductase) and complex III (cytochrome bc_1 complex) [12–14]. The catalytic mechanism of complex III is the protonmotive Q-cycle [15]. For a long time, a semiquinone formed as an intermediate during the oxidation of ubiquinol by complex III has been postulated as the reductant for oxygen converting it to superoxide [16–18]. However, mechanistic studies revealed that this intermediate, if at all is only formed at very low occupancy [19–22] rendering this mechanism very unlikely. An alternative mechanism was deduced from the observation that the production of ROS by antimycin A inhibited complex III increases with the fraction of oxidized quinone reaching a maximum at about 70% reduction of the pool, suggesting that superoxide is primarily formed in a reverse reaction involving transient reduction of ubiquinone by heme b_L [9]. This hypothesis was supported by independent results suggesting that reduced heme b_L was required for superoxide formation by complex III [23,24]. These two opposing mechanisms are in the focus of an ongoing discussion (overview in [25]).

To investigate these ideas we developed a mathematical model for complex III that describes in detail the reactions of the protonmotive Q-cycle, the influence of the membrane potential and the production of superoxide. The aim was to design a model that was (i) detailed enough to reproduce the effect of the addition of various inhibitors, changes of pH or membrane potential $\Delta\Psi$, as well as different metabolic states (*e.g.* variations of protein quantities occurring in different tissues or young *vs.* old organisms), and (ii) simple enough to be extended by and incorporated into more general models.

1.1. The protonmotive Q-cycle

At complex III, the electrons are transferred from QH_2 to cytochrome *c* in a sophisticated process, called protonmotive Q-cycle [15,26]. In summary (see Fig. 1) two QH_2 molecules pass through complex III, one is oxidized to Q while the other is formally first oxidized to Q and

* Corresponding author.
E-mail address: edda.klipp@rz.hu-berlin.de (E. Klipp).
[1] Present address: Department of Anesthesiology, Intensive-Care Medicine and Pain Therapy, Medical School, Johann Wolfgang Goethe-University, Frankfurt am Main, Germany.

http://dx.doi.org/10.1016/j.bbabio.2014.05.358
0005-2728/

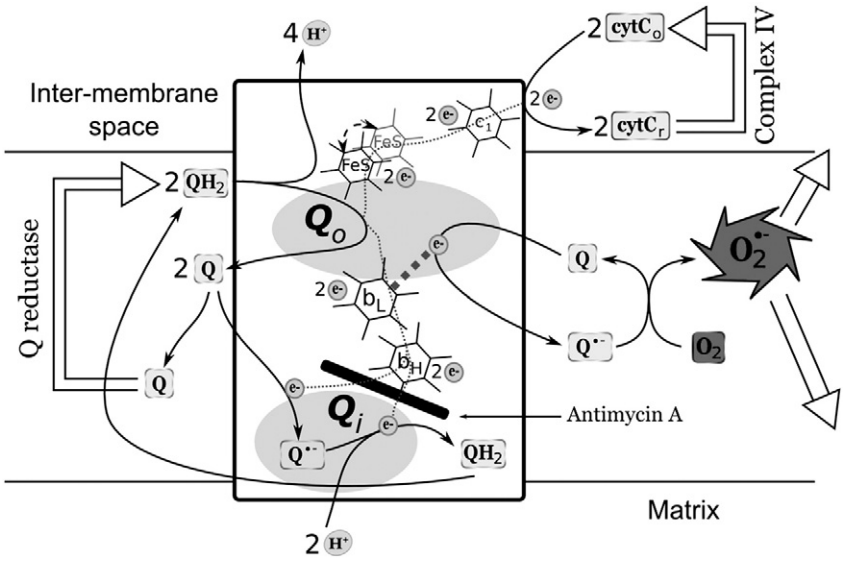

Fig. 1. The protonmotive Q-cycle starts with two electrons entering complex III. QH_2 gives one electron to FeS (which is eventually transferred to cytochrome *c via* heme c_1) and a second electron reduces heme b_L. This electron is transferred to an oxidized quinone at the Q_i site *via* heme b_H. The semiquinone then remains there, stabilized by b_H. Next a second QH_2 gives its electrons to complex III at the Q_o site (as before, one goes to FeS, and one to b_L); the second electron reduces the semiquinone waiting at the Q_i site, which then takes up two protons from the matrix to form QH_2. The model describes superoxide production *via* an electron flow from reduced heme b_L to Q and then onto oxygen leading to the formation of superoxide [9].

then reduced back to QH_2. In the first step a fully reduced ubiquinone diffuses to the Q_o site, located at the outer side of the inner mitochondrial membrane where it is assumed to be oxidized in a concerted mechanism [20,21,27]. The first electron goes to the "Rieske" iron–sulfur cluster and the second to heme b_L. During this reaction, two protons are released into the inter-membrane space.

The hydrophilic domain of the reduced "Rieske" iron–sulfur protein moves from a position near heme b_L to a position near the heme center of cytochrome c_1. The electron is transferred to cytochrome c_1 and the oxidized FeS returns to its original position, ready to receive again an electron from another ubiquinol.

Meanwhile an oxidized ubiquinone, Q, enters the Q_i site, waiting to be reduced. This becomes possible after the reduced heme b_L transfers its electron to the oxidized heme b_H from where it moves onto an oxidized ubiquinone at the Q_i site. The resulting ubisemiquinone is stabilized by b_H [28], waiting for a second electron. This additional electron comes from a second ubiquinol entering the Q_o site, which gives its electrons to the iron–sulfur cluster and heme b_L, as in the first half-cycle. Again the electron is passed from b_L to b_H and then to the semiquinone waiting at the Q_i site. This last process involves the uptake of two protons from the matrix to form a fully reduced quinone QH_2.

Per round of Q-cycle, this results in the formation of two reduced cytochrome *c*, together with the generation of one Q. Additionally, four protons are released into the inter-membrane space, while two protons are taken up from the matrix. That means just looking at complex III only two charges cross the membrane and this is the pump stoichiometry energetically relevant for its contribution to the formation of the protonmotive force. The two additional protons released to the intermembrane space by complex III are "scalar", *i.e.* they do not contribute to the vectorial charge translocation as such, although – together with the protons taken up during reduction of ubiquinone by the dehydrogenase – they are important to balance the overall stoichiometry of chemical protons.

$$QH_2 + 2cytC_{ox} + 2H^+_{MX} \rightleftharpoons Q + 2cytC_{red} + 4H^+_{IMS}.$$

Since the initial proposal of the protonmotive Q-cycle [15], modifications have been proposed to explain the experimental data gathered over the years [29]. The double-gating theory has been introduced to avoid short-circuits in the model that are not seen experimentally [30,31]. In the model presented here, we avoid short-circuits by assuming a concerted mechanism for the quinone oxidation at complex III: QH_2 releases both electrons effectively at the same time and no transfer between bL and FeS is allowed. Reverse electron transfers (and so QH_2 production at Q_o) are only possible if b_L and FeS are reduced.

Over the last years several models of the respiratory chain have been developed [32–35], but only a few address the question of superoxide production by complex III [36–40]. Unfortunately, all models allow for the presence of a semiquinone at Q_o when at the same time b_L is in its reduced form. But this situation is quite improbable due to electrostatic considerations [19]. Additionally, there are several points that render the existing models unsuitable for us. Selivanov's model [36] comprises more than 400 state variables representing the different electronic configurations of complex III, making it quite complex and difficult to handle. Quinlan's model [39] focuses on Q_o reactions, and only addresses complex III inhibition by antimycin A. And Demin's model [41,38] not only considers the quinone oxidation at the Q_o site as a two step reaction, but also omits the existence of a semiquinone at the Q_i site.

A recent, thermodynamically consistent, simple model with only 6 state variables [40] could be nicely fitted to experimental data of turnover rates of the bc_1 complex. However, its simplicity makes it unsuitable to test our hypothesis, since the positions of electrons at the Q_o site are not determined.

Thus, we developed a new model to set a different focus and to avoid some shortcomings of previous models. Precisely, we incorporated the hypothetical mechanism of ROS production by complex III involving reverse electron transfer from heme b_L to oxygen *via* oxidized ubiquinone [9].

2. Material and methods

2.1. Units

All concentrations are expressed in mol per L. The kinetic constant units depend on the reactions considered: $mol^{1-A} \cdot L^{A-1} \cdot s^{-1}$, with *A* the sum of the orders of the species. $\Delta\Psi$ is in mV, with $\Delta\Psi = \Psi_{IMS} - \Psi_{MX}$, where *IMS* denotes inter-membrane space, and *MX* the matrix.

2.2. Structure of the model

The components taken into account in the model are: complex III, cytochrome *c* and the quinone pool. All other components of the respiratory chain are not in the scope of this study.

In order to keep the model tractable, we focus on the following three centers of complex III: the iron–sulfur cluster (FeS), heme b_L and heme b_H. Heme c_1 has been neglected.

The following notation is introduced to describe the reactions taking place in the model. The different centers of complex III (FeS, b_L, b_H) can be in two different states: reduced (r) or oxidized (o). The symbol * stands for any of the two possible states. For example, CIII(r,o,*) refers to a configuration of complex III with FeS reduced (r), b_L oxidized (o), and b_H reduced or oxidized (*). Furthermore, the subscript "*MX*" indicates a matrix location while "*IMS*" indicates the inter-membrane space. Using this notation the model can be described by the following six equations.

1. Reduced ubiquinone transfers its two electrons to complex III, if both FeS and b_L are oxidized:

$$\mathrm{CIII}(o,o,*) + \mathrm{QH_2} \rightleftharpoons \mathrm{CIII}(r,r,*) + \mathrm{Q} + 2\mathrm{H}^+_{IMS}.$$

2. Heme b_L passes its electron to heme b_H, if heme b_H is oxidized:

$$\mathrm{CIII}(*,r,o) \rightleftharpoons \mathrm{CIII}(*,o,r).$$

3. At the Q_i site, one electron is transferred from reduced heme b_H ($b_H^{\cdot}$) to oxidized quinone (Q). The resulting semiquinone then forms a stabilizing complex with heme b_H by sharing its electron. This stabilized state is indicated in the equation by dots.

$$\mathrm{CIII}(*,*,r) + \mathrm{Q} \rightleftharpoons \mathrm{CIII}(*,*,o)\cdots \mathrm{Q}^{\cdot -}.$$

4. At the Q_i site, ($b_H^{\cdot}$) can also give one electron to a semiquinone ($Q^{\cdot -}$) if it is present. Two protons from the matrix are consumed to produce QH_2:

$$\mathrm{CIII}(*,*,r)\cdots \mathrm{Q}^{\cdot -} + 2\mathrm{H}^+_{MX} \rightleftharpoons \mathrm{CIII}(*,*,o) + \mathrm{QH_2}.$$

5. Reduced FeS transfers its electron to oxidized cytochrome *c*:

$$\mathrm{CIII}(r,*,*) + \mathrm{cytC} \rightleftharpoons \mathrm{CIII}(o,*,*) + \mathrm{cytC}^{\cdot}.$$

6. As proposed [9] reduced heme b_L ($b_L^{\cdot}$) may donate one electron to Q to transiently produce $Q^{\cdot -}$ at the Q_o site that is then oxidized by O_2 to generate superoxide ($O_2^{\cdot -}$):

$$\mathrm{CIII}(*,r,*) + \mathrm{Q} \rightleftharpoons \mathrm{CIII}(*,o,*) + \mathrm{Q}^{\cdot -}$$
$$\mathrm{Q}^{\cdot -} + \mathrm{O_2} \rightarrow \mathrm{Q} + \mathrm{O_2}^{\cdot -}.$$

The constants for the six reactions are k_1 to k_6 (forward reactions) and k_{-1} to k_{-6} (backward reactions), respectively. In our model complex III has sixteen possible electronic configurations, A–P (see Fig. 2); eight for complex III alone, and eight for complex III bound to $Q^{\cdot -}$. This leads to the model structure presented by Fig. 2.

In our model the concentrations of some variables are kept constant. This holds for the membrane potential $\Delta\Psi$, the oxygen concentration, cytochrome *c* as well as the ratio of oxidized *vs.* reduced quinone. Therefore the total rate of cytochrome *c* reduction can be calculated by the summation of all fluxes involving reaction 5 and the rate of superoxide production is calculated by summing up all fluxes involving reaction 6. The explicit system of ODEs is given in Appendix A.

2.3. Modeling antimycin A inhibition

Antimycin A is an inhibitor of complex III, commonly used to study details of ROS generation at this complex. It binds complex III at the Q_i site, preventing the quinone to enter this site. In the presence of antimycin A, electrons are accumulating at hemes b_L and b_H. The reduction of quinone at the Q_o site by heme b_L is then favored [9] leading to superoxide formation. In modeling terms this means that reactions 3 (forward) and 4 (backward) are blocked during antimycin A treatment.

2.3.1. Inhibition of cytochrome c reduction by an occupied Q_i site

Recently a mechanism has been proposed to explain the phenomenon that the rate of complex III changes if the Q_i site is occupied by a molecule [42]. This idea provides a mechanistic basis for early postulates that the antimycin A binding site and the Rieske protein are conformationally linked [43,44]. It is known that the Q_i and Q_o sites are connected *via* a helix. The author hypothesized that the movement of FeS from heme b_L to cytochrome c_1 is influenced by this helix. If the helix is mobile, then FeS can move freely, but if the helix is fixed, the movement of FeS is restricted. If the Q_i site is not occupied, the helix is mobile, but if Q_i is occupied by antimycin A or a semiquinone attached near heme b_H, the helix is fixed and the movement of FeS is restricted.

To incorporate this idea in the model, the rate constants k_5 and k_{-5} are modified by $inhib_{k5}$ in the presence of antimycin A or of a stabilized semiquinone at the Q_i site:

$$\begin{cases} k_5' = k_5 \cdot inhib_{k5}, & \text{for} \quad [\mathrm{CIII}(*,*,*)\cdots \mathrm{Q}^{\cdot -}] \\ k_5' = k_5, & \text{else} \end{cases} \tag{1}$$

and

$$\begin{cases} k_{-5}' = k_{-5} \cdot inhib_{k5}, & \text{for} \quad [\mathrm{CIII}(*,*,*)\cdots \mathrm{Q}^{\cdot -}] \\ k_{-5}' = k_{-5}, & \text{else} \end{cases} \tag{2}$$

2.3.2. Effect of the oxidation state of heme b_H

In a previous model, the effects of the oxidation state of heme b_H on ROS production were modeled, if complex III is inhibited [39]. A factor was used to slow down the oxidation of the semiquinone at the Q_o site when heme b_H is reduced. In our model we implemented a similar mechanism by applying an inhibition (*via* $inhib_{k6}$) to reaction 6 (semiquinone formation with an electron from heme b_L, see Fig. 2) for those species of complex III that have a reduced heme b_H (species D, H, J and N). The same formalism was applied as for the inhibition of reaction 5 (see Eqs. (1) and (2)).

2.4. Equations of the model

Every electron transfer is modeled using mass-action kinetics, the global rate υ of the reaction is:

$$\upsilon = k_f \cdot \prod_i [S_i]^{n_i} - k_b \cdot \prod_j \left[P_j\right]^{n_j} \tag{3}$$

where n_i and n_j denote the respective molecularities of substrates and products in this reaction. The transfer of electrons between b_L and b_H (reaction 2) is the only reaction significantly influenced by $\Delta\Psi$ [29]. Therefore we define new rate constants, $k_{2,\Delta\Psi}$ and $k_{-2,\Delta\Psi}$, which depend on the value of $\Delta\Psi$ according to [45] and [46]:

$$k_{2,\Delta\Psi} = k_2 \cdot e^{-\delta\cdot\alpha\cdot\frac{\Delta\Psi\cdot F}{RT}} \tag{4}$$

$$k_{-2,\Delta\Psi} = k_{-2} \cdot e^{\delta\cdot(1-\alpha)\cdot\frac{\Delta\Psi\cdot F}{RT}}. \tag{5}$$

For $\Delta\Psi = 0$ these expressions simplify to k_2 and k_{-2}. δ is the fraction of the membrane potential that affects the transfer, and α is the fraction

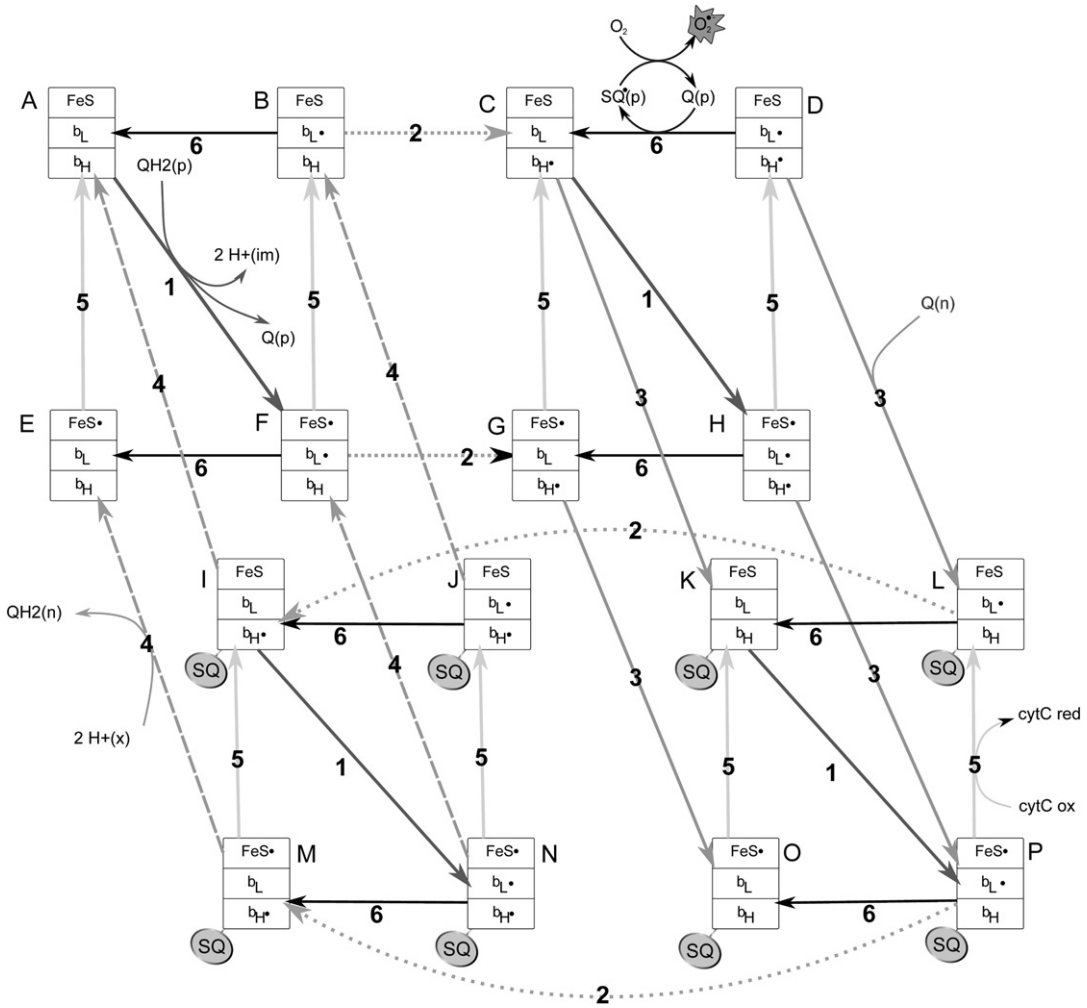

Fig. 2. Model of complex III. The 16 electronic configurations of complex III (A to P) are depicted as rectangles with three boxes, representing the redox-centers. The dots next to the center represent the presence (or absence) of an electron. The states I to P contain a semiquinone stabilized at the Q_i site. The six electron transfers of the model (see text) are represented by arrows and labeled with numbers. 1: reduction of complex III by QH_2 (two electrons are transferred); 2: transfer of the electron from heme b_L to heme b_H (dotted arrows); 3: reduction of quinone at Q_i; 4: final reduction of $Q^{\cdot -}$ at Q_i (dashed arrows); 5: reduction of cytochrome *c* by *FeS*. 6: transient production of semiquinone at Q_o site and reduction of oxygen.

of the membrane potential affecting the forward reaction. α is set to 0.5, considering that the membrane potential affects both forward and backward reactions equally. δ is set to 0.8, as reaction 2 is the major reaction affected by $\Delta\Psi$. The effect of $\Delta\Psi$ on the reactions 1, 3 and 4 were neglected after testing the same equation with δ equal to 0.1.

2.5. Parameterizing the model

To perform actual simulations of the model, numerical values have to be assigned to the various parameters. This is done in a three-step procedure.

In the first approximation rate constants for reactions 1 to 6 (which have a suitable kinetics) are calculated using electron tunneling rate equations [47,48]. This provides starting values for the next step that are in a physiologically relevant area of the parameter space.

In a second phase, these parameter values are optimized using the genetic fitting algorithm of Copasi [49] (number of generations: 2000; population size: 200; random number generator: 1; seed: 0) followed by a local algorithm (Levenberg and Marquardt; iteration limit 200; tolerance: 1×10^{-5}) of Copasi.

The parameters were fitted to experimental data [50] consisting of respiration rates for complex III during state 3 as well as quinone and cytochrome *c* ratios (reduced to total quantities).

Finally, rate constants were also fitted to a set of experimental data obtained in the presence of antimycin A [39]. The fitting procedure was repeated and generated a second set of parameters.

The parameters $k_{f,6}$ and $k_{r,6}$ (reduction of quinone by b_L) are then injected into the first model (no antimycin A) and to calculate ROS production. They had no effect on the previous fit.

The final parameter values are summarized in Table 1.

3. Results

3.1. Rate of complex III during state 3 respiration

The respiratory rates of coupled mitochondria were measured during state 3 respiration in various organs of the rat: muscle, heart, liver, kidney, and brain [50]. Additionally, the fractions (reduced species to total species) and absolute quantities of quinone and cytochrome *c* were measured, together with the amount of complex III. Considering that these experimental data were obtained under steady-state conditions, the rate of respiration (oxygen consumption by complex IV), corresponding to the rate of cytochrome *c* oxidation by complex IV (four cytochrome *c* for one O_2), can be converted into a rate of production of reduced cytochrome *c* by complex III. We used these data to fit the model parameters. The results are presented in Fig. 3. Except for liver the fit is in good agreement with the experimental results. Since

Table 1
Parameters of the model together with a short description and the values obtained after fitting to experimental data. Two sets of fitted values are given, one obtained without any inhibitor [50] and one obtained in the presence of antimycin A [39].

Name (units)	Description	Values after fitting	
		no Ant. A	w. Ant. A
$k_{f,1}$ (M^{-1} s^{-1})	Rate constants for QH_2 oxidation at Q_o	2.8×10^{11}	1.0×10^{4}
$k_{r,1}$ (M^{-3} s^{-1})		6.2×10^{12}	8.7×10^{10}
$k_{f,2}$ (s^{-1})	Rate constants for electron transfer from b_L to b_H	7.6×10^{8}	1.1×10^{3}
$k_{r,2}$ (s^{-1})		2.9×10^{3}	3.8×10^{1}
$k_{f,3}$ (M^{-1} s^{-1})	Rate constants for the first Q reduction at Q_i	2.0×10^{11}	0
$k_{r,3}$ (s^{-1})		1.3×10^{10}	–
$k_{f,4}$ (M^{-2} s^{-1})	Rate constants for the second Q reduction at Q_i	4.2×10^{18}	–
$k_{r,4}$ (M^{-1} s^{-1})		4.5×10^{-3}	0
$k_{f,5}$ (M^{-1} s^{-1})	Rate constants for the cyt *c* reduction by complex III	2.0×10^{4}	2.2×10^{6}
$k_{r,5}$ (M^{-1} s^{-1})		9.8×10^{2}	6.5×10^{3}
$k_{f,6}$ (M^{-1} s^{-1})*	Rate constants for the reduction of the quinone by b_L	4.9×10^{6}	4.9×10^{6}
$k_{r,6}$ (M^{-1} s^{-1})*		4.0×10^{9}	4.0×10^{9}
$k_{f,7}$ (M^{-1} s^{-1})**	Rate constant for the production of superoxide	2.2×10^{7}	
$inhib_{k_5}$***	Inhibition factor for cyt *c* reduction	6.0×10^{-1}	
$inhib_{k_6}$	Inhibition factor for quinone reduction at Q_o	1	4.8×10^{-1}

* These values are obtained from the second optimization procedure. They are then injected into the model without antimycin A; see text.
** This value has been calculated using the electron tunneling equation; see text.
*** This value applies only when quinone or antimycin A is present at Q_i; see text.

liver mitochondria are often significantly contaminated by other metabolic enzymes and most notably by microsomes that contain large amounts of cytochrome P450 monooxygenases this deviation may reflect an experimental artifact.

Fig. 4A summarizes the results of a typical simulation. The three centers of complex III can each exist in a reduced or oxidized state. Furthermore, heme b_H can either be associated with a semiquinone or not, resulting in a total of 16 different states, numbered from A to P. Arrows indicate the different reactions occurring between these states, where the type of arrow reflects to which of the six general reactions it belongs. The reaction type is also indicated by a number next to the arrow.

The thickness of the arrows indicates the magnitude of the flux through this reaction and a dark background indicates the states with a high steady state occupancy (states without a background have a concentration approaching 0). It can be seen that a reduction of FeS and heme b_L (reaction 1) occurs mainly if no semiquinone is attached to the complex (see Fig. 4).

3.2. Complex III inhibition by antimycin A

Antimycin A is a common inhibitor used in studies of complex III function and its production of ROS. The presence of antimycin A prevents the binding of quinone at the Q_i site. In the model, the effects of antimycin A treatment are simulated by completely inhibiting the forward rate of reaction 3 (formation of semiquinone at the Q_i site) and the backward rate of reaction 4 (production of ubiquinol at the Q_i site) (see Fig. 2). We simulated the effects of a complete inhibition of complex III by antimycin A, since a partial inhibition would lead to reaction shortcuts between the two complex III molecules forming a complex III homodimer [51]. The simulation shows that the concentrations of species I to P and the rates of reactions 3 and 4 drop to zero under antimycin A treatment (Fig. 4B).

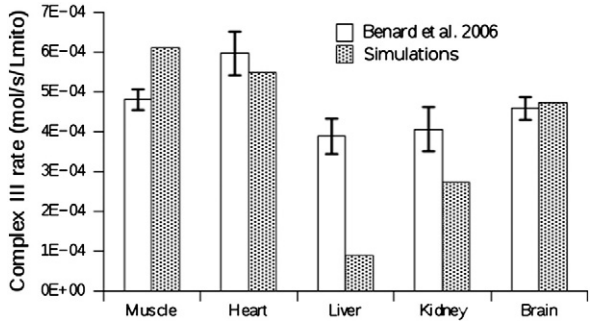

Fig. 3. Comparison of experimental data [50] and model output after fitting. The model (gray bars) was fitted to state 3 electron transfer rates (white bars) for different organs of the rat. pH_{IMS} was set to 7.1, pH_{MX} to 7.2 and $\Delta\Psi$ to 150 mV.

3.3. The ratio of reduced to total Q

It has been shown experimentally that during antimycin inhibition the ratio of reduced quinone to total quinone has a large influence on the ROS production rate [39,9]. ROS generation is maximal at an intermediate fraction and is minimal if the Q-pool is fully oxidized or reduced.

Our model simulations show that the antimycin dependent parameter modification, which we introduced in Section 2.3.1, is essential to reproduce the "bell-shaped" curve describing the dependency of ROS production on the ratio of reduced quinone. The model provides an excellent fit to the ROS generation data (Fig. 5), and also to the measured values for the ratio of reduced b_L (Fig. 5B). Data points are shown as crosses and the results of our fitted model are shown as a continuous line in the diagrams.

3.3.1. ROS production during antimycin treatment

Fig. 4B shows the fluxes and steady state concentrations of the different states of complex III during antimycin A treatment. The total flux, and thus the reduction rate of cytochrome *c* is greatly reduced and the remaining flux is concentrated along the reactions shown in red.

Thus, according to the model simulations the production rate of ROS should be equal to the rate of cytochrome *c* reduction under this condition. Of course this only holds for the rate of cytochrome *c* reduction by slow turnover of the Q_o site occurring, when electrons leak onto oxygen from heme b_L, and not the rate of cytochrome *c* reduction resulting from possible reactions with superoxide. A previous work showed that the antimycin A resistant cytochrome *c* reduction can only be partially suppressed by the addition of excess superoxide dismutase (SOD) [17], indicating that superoxide dependent as well as independent pathways are involved in cytochrome *c* reduction under these conditions.

Our simulations differ from these results, since the model does not include a reaction between cytochrome *c* and superoxide. If it were included, 50% of the cytochrome *c* reduction would stem from a reaction with superoxide and could thus be abolished by SOD. This agrees reasonably well with the 35% observed experimentally [17]. The discrepancies here may be due to short-circuits occurring at low rate that are ignored by this model.

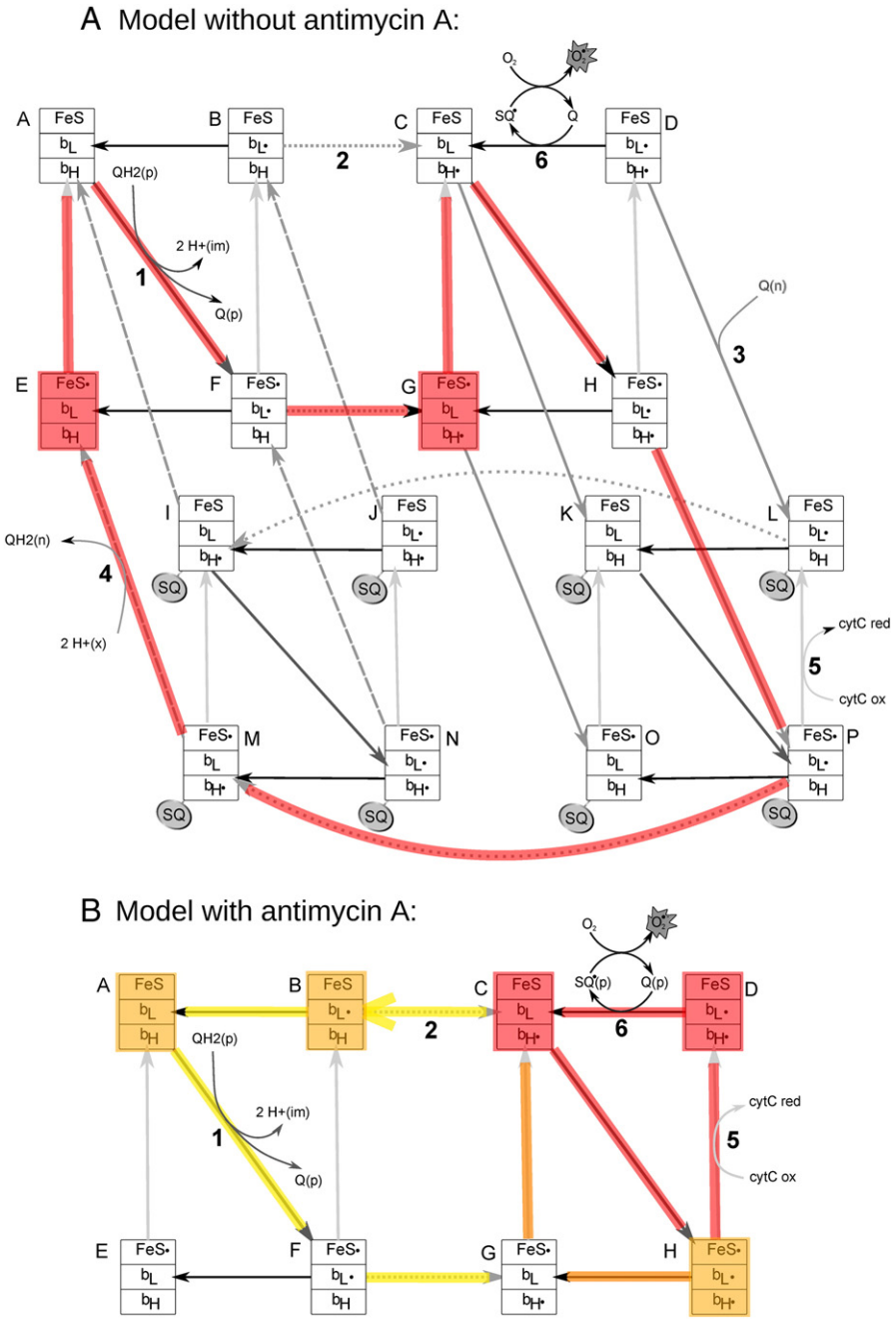

Fig. 4. States of complex III and the protonmotive Q-cycle during (A) state 3 respiration and (B) antimycin A inhibition. The states with the highest steady state occupancy, as well as the reactions with the highest flux are highlighted in color. Occupancies/rates shown in red are about ten times higher than those shown in yellow.

3.4. Combined effect of the fraction of reduced Q and ΔΨ

ΔΨ not only plays a central role in ATP generation, apoptosis and mitophagy [52], but also greatly influences ROS production. After we confirmed that our model can reproduce experimental findings very well for $\Delta\Psi = 0$ (Fig. 5), we next calculated ROS generation rates with and without antimycin A for values of ΔΨ ranging from 0 to 250 mV (Fig. 6).

The calculated ROS production exhibits an exponential dependence on ΔΨ if complex III is not inhibited by antimycin A. This dependence is the direct result of the modulation of the rate of reaction 2 by ΔΨ, and the fraction of reduced b_L. This is qualitatively and quantitatively validated by independent experimental data, where superoxide production is measured against membrane potential [53]. Both, model calculations and experimental data exhibit a 4-fold increase in ROS production (from $6.2 \cdot 10^{-7}$ to $2.6 \cdot 10^{-6}$ mol s^{-1} for the model) for a rise in ΔΨ from 150 to 200 mV (Q ratio = 0.05). In addition, the simulations show that this effect is most pronounced for small fractions of reduced quinone, *i.e.* for fractions that are also biologically relevant [50]. Under these conditions the concentration of oxidized quinone at Q_o is especially high, maximizing the reaction rate between reduced b_L and quinone.

But ΔΨ has no influence on the ROS production if complex III is inhibited by antimycin A. Under this condition the flux of electrons from b_L to b_H is practically blocked and since this is the place where ΔΨ exerts its effect, antimycin A diminishes the effect of the membrane potential on the ROS production.

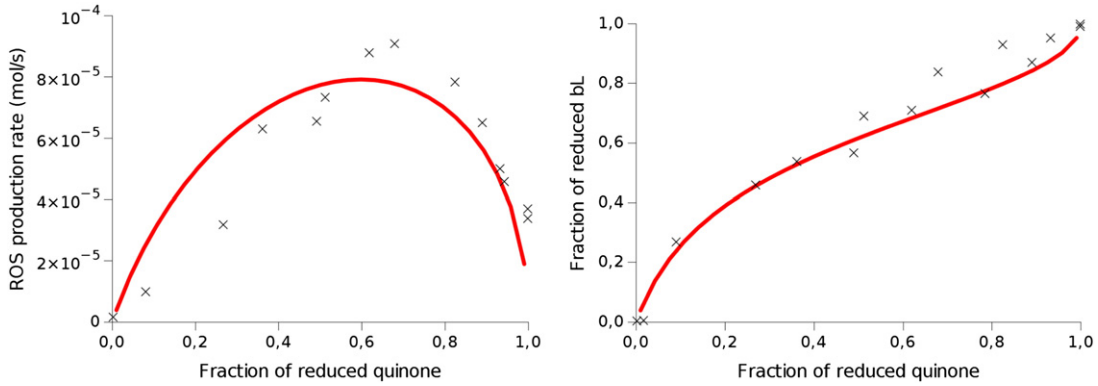

Fig. 5. Comparison of experimental data [39] (Fig. 1) and the model output after parameter fitting. The ROS production rate (left) and fraction of reduced heme b_L (right) as a function of the fraction of reduced quinone is shown. The substrate concentrations of the experimental data were converted to levels of reduced quinone using the Nernst equation. An apparent E^0 was determined for glutamate/malate assuming that maximal ROS production occurred at the same Q ratio for both conditions.

4. Discussion

We present a model of the electron transfers inside complex III, featuring ROS production and concerted electron transfer at the Q_o site, which is mathematically tractable and is in good quantitative agreement with experimental results.

Furthermore, the model can simulate complex III under normal conditions as well as under inhibition by antimycin A and in the presence of an increasing membrane potential.

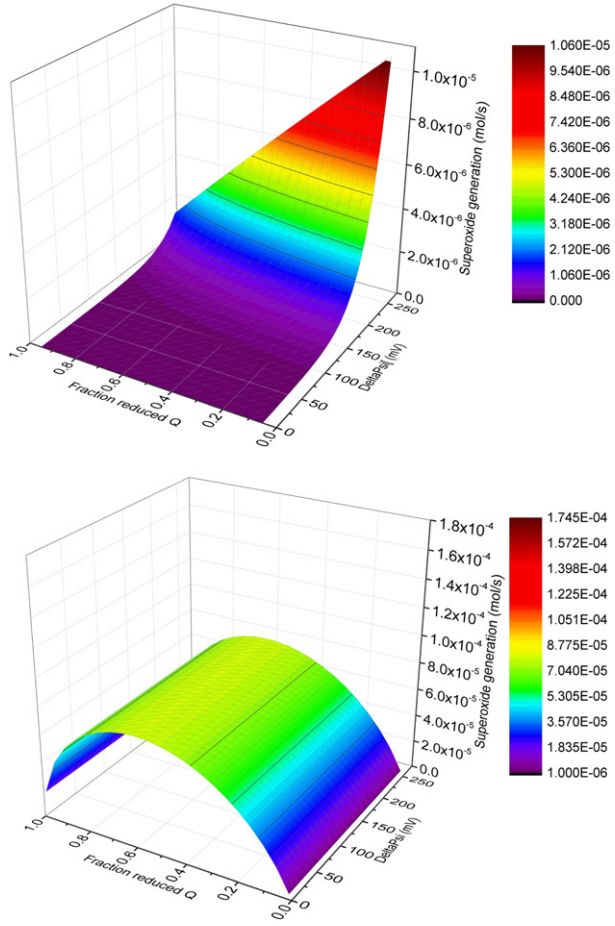

Fig. 6. Calculation of ROS production as a function of ΔΨ and the fraction of reduced quinone, without (top) and with antimycin A (bottom). Since antimycin A blocks the electron transfer from b_H to ubiquinole, the membrane potential has practically no influence on the radical production.

4.1. Simplifications

To keep the mathematical description compact and tractable a couple of simplifications were applied to reduce the number of possible states of complex III.

Several earlier models assume a sequential, two step, mechanism at the Q_o site [39,36,54,48]. This can lead to states that are unlikely to exist, such as the presence of a semiquinone at Q_o close to a reduced heme b_L [19]. So far such a semiquinone has only been observed under very artificial conditions [55,56] that are not relevant for our model. Therefore, complex III reduction by QH_2 was assumed to be a (quasi) concerted reaction. This approach has the added benefit that it eliminates shortcut reactions that would have to be considered otherwise (see [30,31]).

The competition of different quinone species for the Q_o site has not been implemented in the present model, since this would greatly increase the number of possible states. Already a distinction between free or occupied by either QH_2 or Q would lead to 48 possible states.

4.2. Parameter choice

To reproduce the different data sets, two sets of parameters were used, one for normal complex III behavior and one for complex III inhibited by antimycin A. This distinction between a "normal" model and an "antimycin" model was expected, since antimycin A is suspected to change the electron transfer kinetics within complex III.

4.3. Quinone and ROS production

Our model probes the concept that oxidized quinone is needed as a redox mediator between heme b_L and molecular oxygen. Even without the formation of a semiquinone during the reduction of complex III by QH_2, the presented model is able to reproduce the bell-shape curve of the ROS production rate with antimycin A, and the rate of cytochrome *c* reduction during state 3 of respiration.

The curves for ROS production during antimycin A treatment as given by [9] and [39] are similar (*i.e.* bell shaped) but their maximum is seemingly at a different quinone ratio (70% *vs.* 30%). However, after converting the substrate concentrations given by [39] (Fig. 1) into fractions of reduced quinone using the Nernst equation, it turns out that both studies find a maximum ROS generation at 70% reduced quinone. For our modeling study we chose the data set that contained more data points [39].

The model simulations show that the level of semiquinone always remains very low in comparison to other model species (with and without antimycin A). For instance, the semiquinone steady state level is roughly 1000 times lower than the total quinone concentration (between 10^{-9} and 10^{-7} M depending on the experiments, *vs.* mM for the other quinones). Thus, our model is in agreement with experiments

where no, or only in extreme situations, semiquinone was detected at the Q_o site.

4.4. Role of $\Delta\Psi$ in ROS production

The membrane potential plays an important role for the respiratory chain and in the mitochondrial metabolism. Its value affects the rate of ATP production and for extremely high values can even lead to a reverse electron flow in the respiratory chain complexes [57]. Additionally, it has been recently shown that mitochondria with low $\Delta\Psi$ are more likely to be degraded by mitophagy [58].

We used this model to explore the effects of $\Delta\Psi$ on ROS production under various conditions, especially regarding the fraction of reduced quinone. Fig. 6 shows the rate of ROS generation as a function of $\Delta\Psi$ and the fraction of reduced ubiquinone under normal conditions and during inhibition by antimycin A.

Without antimycin A, ROS generation at complex III is proportional to the fraction of reduced quinone, but is mostly controlled by $\Delta\Psi$ (exponential increase with $\Delta\Psi$), which agrees well with experimental data [53]. With antimycin A treatment the situation is different in that $\Delta\Psi$ is much less influential in controlling ROS generation. Antimycin A blocks the flow of electrons from b_H to ubiquinole, leading to the accumulation of reduced b_H. Since the flow of electrons from b_L to b_H is the main reaction influenced by the membrane potential, ROS production is largely independent of the $\Delta\Psi$ under antimycin A treatment. Instead, under this condition it is the fraction of reduced quinone that plays the major role in controlling ROS production.

Most of the mitochondria in the different organs of the rat have a low fraction of ubiquinol [50]. This prevents superoxide formation by complex III in the presence of antimycin A. But without antimycin A, a low ubiquinol fraction together with an increase of $\Delta\Psi$ leads to a rise of the superoxide production. Since superoxide released from the Q_o site into the inter-membrane space has been proposed to be involved in ROS signaling, in particular under conditions of pharmacological and hypoxic preconditioning [59–62], this observation has two important implications, namely that ROS signaling by complex III exponentially increases with $\Delta\Psi$, but also critically depends on the redox state of the ubiquinone pool. Remarkably, at a given membrane potential ROS production is maximal with a low fraction of reduced ubiquinone and approaches very low levels if the Q-pool is fully reduced.

5. Conclusion

Our model studies the electron flow inside complex III that leads to ROS production.

The model reinforces the hypothesis that superoxide formation by complex III involves ubiquinone as a redox mediator between cytochrome b_L and oxygen [9]. In particular, no semiquinone intermediate of the protonmotive Q-cycle at the Q_o site is required to reproduce the experimental data.

We also implemented the idea that interactions between antimycin A and complex III lead to modifications of the electron transfers far from the Q_i site where antimycin A acts. This lead to simulation results that agree very well with experimental findings. However, the molecular mechanisms for such an interaction remain to be elucidated. These may be mechanical, as proposed by [42], or electronic [39].

Acknowledgements

This work was funded by the German Federal Ministry for Education and Research (BMBF) through the *GerontoMitoSys* project (FKZ 0315584) to EK and UB. The work of SD and UB was also supported by the Deutsche Forschungsgemeinschaft (SFB815 "*Redox Regulation: Generator systems and functional consequences*", project A02).

Appendix A

The model shown in fig. 2 leads to the following system of 16 coupled ordinary differential equations, which are based on reversible mass action kinetics.

$$\frac{dA}{dt} = -\left(k_{f,1}A\ QH_2 - k_{r,1}F\ Q\ H_{IM}^{+2}\right) + \left(k_{f,4}I\ H_x^{+2} - k_{r,4}A\ QH_2\right) + \left(k_{f,5}E\ cytC_{ox} - k_{r,5}A\ cytC_{red}\right) + \left(k_{f,6}B\ Q - k_{r,6}A\ Q^{\bullet}\right) \quad (1)$$

$$\frac{dB}{dt} = -\left(k_{f,2}B - k_{r,2}C\right) + \left(k_{f,4}J\ H_x^{+2} - k_{r,4}B\ QH_2\right) + \left(k_{f,5}F\ cytC_{ox} - k_{r,5}B\ cytC_{red}\right) - \left(k_{f,6}B\ Q - k_{r,6}A\ Q^{\bullet}\right) \quad (2)$$

$$\frac{dC}{dt} = -\left(k_{f,1}C\ QH_2 - k_{r,1}H\ Q\ H_{IM}^{+2}\right) + \left(k_{f,2}B - k_{r,2}C\right) - \left(k_{f,3}C\ Q - k_{r,3}K\right) + \left(k_{f,5}G\ cytC_{ox} - k_{r,5}C\ cytC_{red}\right) + \left(k_{f,6}D\ Q - k_{r,6}C\ Q^{\bullet}\right) \quad (3)$$

$$\frac{dD}{dt} = -\left(k_{f,3}D\ Q - k_{r,3}L\right) + \left(k_{f,5}H\ cytC_{ox} - k_{r,5}D\ cytC_{red}\right) - \left(k_{f,6}D\ Q - k_{r,6}C\ Q^{\bullet}\right) \quad (4)$$

$$\frac{dE}{dt} = \left(k_{f,4}M\ H_x^{+2} - k_{r,4}E\ QH_2\right) - \left(k_{f,5}E\ cytC_{ox} - k_{r,5}A\ cytC_{red}\right) + \left(k_{f,6}F\ Q - k_{r,6}E\ Q^{\bullet}\right) \quad (5)$$

$$\frac{dF}{dt} = \left(k_{f,1}A\ QH_2 - k_{r,1}F\ Q\ H_{IM}^{+2}\right) - \left(k_{f,2}F - k_{r,2}G\right) + \left(k_{f,4}N\ H_x^{+2} - k_{r,4}F\ QH_2\right) - \left(k_{f,5}F\ cytC_{ox} - k_{r,5}B\ cytC_{red}\right) - \left(k_{f,6}F\ Q - k_{r,6}E\ Q^{\bullet}\right) \quad (6)$$

$$\frac{dG}{dt} = \left(k_{f,2}F - k_{r,2}G\right) - \left(k_{f,3}G\ Q - k_{r,3}O\right) - \left(k_{f,5}G\ cytC_{ox} - k_{r,5}C\ cytC_{red}\right) + \left(k_{f,6}H\ Q - k_{r,6}G\ Q^{\bullet}\right) \quad (7)$$

$$\frac{dH}{dt} = \left(k_{f,1}C\ QH_2 - k_{r,1}H\ Q\ H_{IM}^{+2}\right) - \left(k_{f,3}H\ Q - k_{r,3}P\right) - \left(k_{f,5}H\ cytC_{ox} - k_{r,5}D\ cytC_{red}\right) - \left(k_{f,6}H\ Q - k_{r,6}G\ Q^{\bullet}\right) \quad (8)$$

$$\frac{dI}{dt} = -\left(k_{f,1}I\ QH_2 - k_{r,1}N\ Q\ H_{IM}^{+2}\right) + \left(k_{f,2}L - k_{r,2}I\right) - \left(k_{f,4}I\ H_x^{+2} - k_{r,4}A\ QH_2\right) + \left(k_{f,5}M\ cytC_{ox} - k_{r,5}I\ cytC_{red}\right) + \left(k_{f,6}J\ Q - k_{r,6}I\ Q^{\bullet}\right) \quad (9)$$

$$\frac{dJ}{dt} = -\left(k_{f,4}J\ H_x^{+2} - k_{r,4}B\ QH_2\right) + \left(k_{f,5}N\ cytC_{ox} - k_{r,5}J\ cytC_{red}\right) - \left(k_{f,6}J\ Q - k_{r,6}I\ Q^{\bullet}\right) \quad (10)$$

$$\frac{dK}{dt} = -\left(k_{f,1}K\ \mathrm{QH_2} - k_{r,1}P\ \mathrm{Q}\ \mathrm{H}_{IM}^{+2}\right) + \left(k_{f,3}C\ \mathrm{Q} - k_{r,3}K\right) + \left(k_{f,5}O\ \mathrm{cytC_{ox}} - k_{r,5}K\ \mathrm{cytC_{red}}\right) + \left(k_{f,6}L\ \mathrm{Q} - k_{r,6}K\ \mathrm{Q^{\bullet}}\right) \quad (11)$$

$$\frac{dL}{dt} = -\left(k_{f,2}L - k_{r,2}I\right) + \left(k_{f,3}D\ \mathrm{Q} - k_{r,3}L\right) + \left(k_{f,5}P\ \mathrm{cytC_{ox}} - k_{r,5}L\ \mathrm{cytC_{red}}\right) - \left(k_{f,6}L\ \mathrm{Q} - k_{r,6}K\ \mathrm{Q^{\bullet}}\right) \quad (12)$$

$$\frac{dM}{dt} = \left(k_{f,2}P - k_{r,2}M\right) - \left(k_{f,4}M\ \mathrm{H}_x^{+2} - k_{r,4}E\ \mathrm{QH_2}\right) - \left(k_{f,5}M\ \mathrm{cytC_{ox}} - k_{r,5}I\ \mathrm{cytC_{red}}\right) + \left(k_{f,6}N\ \mathrm{Q} - k_{r,6}M\ \mathrm{Q^{\bullet}}\right) \quad (13)$$

$$\frac{dN}{dt} = \left(k_{f,1}I\ \mathrm{QH_2} - k_{r,1}N\ \mathrm{Q}\ \mathrm{H}_{IM}^{+2}\right) - \left(k_{f,4}N\ \mathrm{H}_x^{+2} - k_{r,4}F\ \mathrm{QH_2}\right) - \left(k_{f,5}N\ \mathrm{cytC_{ox}} - k_{r,5}J\ \mathrm{cytC_{red}}\right) - \left(k_{f,6}N\ \mathrm{Q} - k_{r,6}M\ \mathrm{Q^{\bullet}}\right) \quad (14)$$

$$\frac{dO}{dt} = \left(k_{f,3}G\ \mathrm{Q} - k_{r,3}O\right) - \left(k_{f,5}O\ \mathrm{cytC_{ox}} - k_{r,5}K\ \mathrm{cytC_{red}}\right) + \left(k_{f,6}P\ \mathrm{Q} - k_{r,6}O\ \mathrm{Q^{\bullet}}\right) \quad (15)$$

$$\frac{dP}{dt} = \left(k_{f,1}K\ \mathrm{QH_2} - k_{r,1}P\ \mathrm{Q}\ \mathrm{H}_{IM}^{+2}\right) - \left(k_{f,2}P - k_{r,2}M\right) + \left(k_{f,3}H\ \mathrm{Q} - k_{r,3}P\right) - \left(k_{f,5}P\ \mathrm{cytC_{ox}} - k_{r,5}L\ \mathrm{cytC_{red}}\right) - \left(k_{f,6}P\ \mathrm{Q} - k_{r,6}O\ \mathrm{Q^{\bullet}}\right) \quad (16)$$

References

[1] D. Harman, Aging: a theory based on free radical and radiation chemistry, J. Gerontol. 11 (3) (1956) 298–300 (URL http://www.ncbi.nlm.nih.gov/pubmed/13332224).

[2] W. Ladiges, J. Wanagat, B. Preston, L. Loeb, P. Rabinovitch, A mitochondrial view of aging, reactive oxygen species and metastatic cancer, Aging Cell 9 (4) (2010) 462–465, http://dx.doi.org/10.1111/j.1474-9726.2010.00579.x (URL http://www.ncbi.nlm.nih.gov/pubmed/20456297).

[3] J. Sastre, F.V. Pallardó, J. Viña, Mitochondrial oxidative stress plays a key role in aging and apoptosis, IUBMB Life 49 (5) (2000) 427–435, http://dx.doi.org/10.1080/152165400410281 (URL http://www.journals.cambridge.org/abstract_S0267190500200135 http://www.ncbi.nlm.nih.gov/pubmed/10902575).

[4] G. Lenaz, Role of mitochondria in oxidative stress and ageing, Biochim. Biophys. Acta 1366 (1–2) (1998) 53–67 (URL http://www.ncbi.nlm.nih.gov/pubmed/9714734).

[5] J. Miquel, An integrated theory of aging as the result of mitochondrial-DNA mutation in differentiated cells, Arch. Gerontol. Geriatr. 12 (2–3) (1991) 99–117 (URL http://www.ncbi.nlm.nih.gov/pubmed/15374442).

[6] A.W. Linnane, S. Marzuki, T. Ozawa, M. Tanaka, Mitochondrial DNA mutations as an important contributor to ageing and degenerative diseases, Lancet 1 (8639) (1989) 642–645 (URL http://linkinghub.elsevier.com/retrieve/pii/S0140673689921454 http://www.ncbi.nlm.nih.gov/pubmed/2564461).

[7] J. Miquel, A.C. Economos, J. Fleming, J.E. Johnson, Mitochondrial role in cell aging, Exp. Gerontol. 15 (6) (1980) 575–591 (URL http://www.ncbi.nlm.nih.gov/pubmed/7009178).

[8] D. Harman, Free radical theory of aging: dietary implications, Am. J. Clin. Nutr. 25 (8) (1972) 839–843 (URL http://www.ncbi.nlm.nih.gov/pubmed/5046729).

[9] S. Dröse, U. Brandt, The mechanism of mitochondrial superoxide production by the cytochrome bc_1 complex, J. Biol. Chem. 283 (31) (2008) 21649–21654, http://dx.doi.org/10.1074/jbc.M803236200 (URL http://www.ncbi.nlm.nih.gov/pubmed/18522938).

[10] H.M. Viola, L.C. Hool, Q_o site of mitochondrial complex III is the source of increased superoxide after transient exposure to hydrogen peroxide, J. Mol. Cell. Cardiol. 49 (5) (2010) 875–885, http://dx.doi.org/10.1016/j.yjmcc.2010.07.015 (URL http://www.ncbi.nlm.nih.gov/pubmed/20688078).

[11] M.P. Murphy, A. Holmgren, N.-G. Larsson, B. Halliwell, C.J. Chang, B. Kalyanaraman, S.G. Rhee, P.J. Thornalley, L. Partridge, D. Gems, T. Nyström, V. Belousov, P.T. Schumacker, C.C. Winterbourn, Unraveling the biological roles of reactive oxygen species, Cell Metab. 13 (4) (2011) 361–366, http://dx.doi.org/10.1016/j.cmet.2011.03.010 (URL http://www.ncbi.nlm.nih.gov/pubmed/21459321).

[12] E. Murphy, C. Steenbergen, Mechanisms underlying acute protection from cardiac ischemia–reperfusion injury, Physiol. Rev. 88 (2) (2008) 581–609, http://dx.doi.org/10.1152/physrev.00024.2007 (URL http://physrev.physiology.org/content/88/2/581.short http://www.pubmedcentral.nih.gov/articlerender.fcgi?artid=3199571&tool=pmcentrez&rendertype=abstract).

[13] M.D. Brand, The sites and topology of mitochondrial superoxide production, Exp. Gerontol. 45 (7–8) (2010) 466–472, http://dx.doi.org/10.1016/j.exger.2010.01.003 (URL http://www.pubmedcentral.nih.gov/articlerender.fcgi?artid=2879443&tool=pmcentrez&rendertype=abstract).

[14] S. Dröse, U. Brandt, Molecular mechanisms of superoxide production by the mitochondrial respiratory chain, Adv. Exp. Med. Biol. 748 (2012) 145–169, http://dx.doi.org/10.1007/978-1-4614-3573-0_6 (URL http://www.springerlink.com/index/10.1007/978-1-4614-3573-0 http://www.ncbi.nlm.nih.gov/pubmed/22729857).

[15] P. Mitchell, The protonmotive Q cycle: a general formulation, FEBS Lett. 59 (2) (1975) 137–139 (URL http://www.ncbi.nlm.nih.gov/pubmed/1227927).

[16] J.F. Turrens, a. Alexandre, a.L. Lehninger, Ubisemiquinone is the electron donor for superoxide formation by complex III of heart mitochondria, Arch. Biochem. Biophys. 237 (2) (1985) 408–414 (URL http://www.ncbi.nlm.nih.gov/pubmed/2983613).

[17] F. Muller, R. Crofts, D. Kramer Antony, Multiple Q-cycle bypass reactions at the Q_o site of the cytochrome bc_1 complex, Biochemistry (2002) 7866–7874, http://dx.doi.org/10.1021/bi025581e (URL http://pubs.acs.org/doi/abs/10.1021/bi025581e).

[18] F.L. Muller, A.G. Roberts, M.K. Bowman, D.M. Kramer, Architecture of the Q_o site of the cytochrome bc_1 complex probed by superoxide production, Biochemistry 42 (21) (2003) 6493–6499, http://dx.doi.org/10.1021/bi0342160 (URL http://pubs.acs.org/doi/abs/10.1021/bi0342160 http://www.ncbi.nlm.nih.gov/pubmed/12767232).

[19] U. Brandt, The chemistry and mechanics of ubihydroquinone oxidation at center P (Q_o) of the cytochrome bc_1 complex, Biochim. Biophys. Acta 1365 (1–2) (1998) 261–268 (URL http://www.ncbi.nlm.nih.gov/pubmed/9693740).

[20] B.L. Trumpower, A concerted, alternating sites mechanism of ubiquinol oxidation by the dimeric cytochrome bc_1 complex, Biochim. Biophys. Acta 1555 (1–3) (2002) 166–173 (URL http://www.ncbi.nlm.nih.gov/pubmed/12206910).

[21] A.R. Crofts, The cytochrome bc_1 complex: function in the context of structure, Annu. Rev. Physiol. 66 (2004) 689–733, http://dx.doi.org/10.1146/annurev.physiol.66.032102.150251 (URL http://www.ncbi.nlm.nih.gov/pubmed/14977419).

[22] J. Zhu, T. Egawa, S.-R. Yeh, L. Yu, C.-A. Yu, Simultaneous reduction of iron–sulfur protein and cytochrome b_L during ubiquinol oxidation in cytochrome bc_1 complex, Proc. Natl. Acad. Sci. U. S. A. 104 (12) (2007) 4864–4869, http://dx.doi.org/10.1073/pnas.0607812104 (URL http://www.pubmedcentral.nih.gov/articlerender.fcgi?artid=1829230&tool=pmcentrez&rendertype=abstract).

[23] A. Borek, M. Sarewicz, A. Osyczka, Movement of the iron–sulfur head domain of cytochrome bc_1 transiently opens the catalytic Q_o site for reaction with oxygen, Biochemistry 47 (47) (2008) 12365–12370, http://dx.doi.org/10.1021/bi801207f (URL http://www.ncbi.nlm.nih.gov/pubmed/18956890).

[24] M. Sarewicz, A. Borek, E. Cieluch, M. Swierczek, A. Osyczka, Discrimination between two possible reaction sequences that create potential risk of generation of deleterious radicals by cytochrome bc_1. Implications for the mechanism of superoxide production, Biochim. Biophys. Acta 1797 (11) (2010) 1820–1827, http://dx.doi.org/10.1016/j.bbabio.2010.07.005 (URL http://www.pubmedcentral.nih.gov/articlerender.fcgi?artid=3057645&tool=pmcentrez&rendertype=abstract).

[25] L. Bleier, S. Dröse, Superoxide generation by complex III: from mechanistic rationales to functional consequences, Biochim. Biophys. Acta 1827 (2013) 1320–1331, http://dx.doi.org/10.1016/j.bbabio.2012.12.002 (URL http://www.ncbi.nlm.nih.gov/pubmed/23269318).

[26] U. Brandt, B. Trumpower, The protonmotive Q cycle in mitochondria and bacteria, Crit. Rev. Biochem. Mol. Biol. 29 (3) (1994) 165–197, http://dx.doi.org/10.3109/10409239409086800 (URL http://www.ncbi.nlm.nih.gov/pubmed/8070276).

[27] M. Sarewicz, M. Dutka, S. Pintscher, A. Osyczka, Triplet state of the semiquinone–Rieske cluster as an intermediate of electronic bifurcation catalyzed by cytochrome bc_1, Biochemistry 52 (37) (2013) 6388–6395, http://dx.doi.org/10.1021/bi400624m (URL http://www.pubmedcentral.nih.gov/articlerender.fcgi?artid=3889490&tool=pmcentrez&rendertype=abstract).

[28] T. Ohnishi, B. Trumpower, Differential effects of antimycin on ubisemiquinone bound in different environments in isolated succinate. cytochrome c reductase complex, J. Biol. Chem. 255 (8) (1980) 3278–3284 (URL http://www.jbc.org/content/255/8/3278.short).

[29] E.A. Berry, M. Guergova-Kuras, L.S. Huang, A.R. Crofts, Structure and function of cytochrome bc complexes, Annu. Rev. Biochem. 69 (2000) 1005–1075, http://dx.doi.org/10.1146/annurev.biochem.69.1.1005 (URL http://www.annualreviews.org/doi/abs/10.1146/annurev.biochem.69.1.1005 http://www.ncbi.nlm.nih.gov/pubmed/10966481).

[30] A. Osyczka, C.C. Moser, P.L. Dutton, Fixing the Q cycle, Trends Biochem. Sci. 30 (4) (2005) 176–182, http://dx.doi.org/10.1016/j.tibs.2005.02.001 (URL http://www.ncbi.nlm.nih.gov/pubmed/15817393).

[31] A. Osyczka, C.C. Moser, F. Daldal, P.L. Dutton, Reversible redox energy coupling in electron transfer chains, Nature 427 (6975) (2004) 607–612, http://dx.doi.org/10.1038/nature02242 (URL http://www.ncbi.nlm.nih.gov/pubmed/14961113).

[32] F. Wu, F. Yang, K.C. Vinnakota, D.A. Beard, Computer modeling of mitochondrial tricarboxylic acid cycle, oxidative phosphorylation, metabolite transport, and electrophysiology, J. Biol. Chem. 282 (34) (2007) 24525–24537, http://dx.doi.org/10.1074/jbc.M701024200 (URL http://www.ncbi.nlm.nih.gov/pubmed/17591785).

[33] D.A. Beard, A biophysical model of the mitochondrial respiratory system and oxidative phosphorylation, PLoS Comput. Biol. 1 (4) (2005) e36, http://dx.doi.org/10.1371/journal.pcbi.0010036 (URL http://www.pubmedcentral.nih.gov/articlerender.fcgi?artid=1201326&tool=pmcentrez&rendertype=abstract).

[34] B. Korzeniewski, The modeling of oxidative phosphorylation in skeletal muscle, Jpn. J. Physiol. 54 (6) (2004) 511–516 (URL http://www.ncbi.nlm.nih.gov/pubmed/15760482).
[35] B. Korzeniewski, J.A. Zoladz, A model of oxidative phosphorylation in mammalian skeletal muscle, Biophys. Chem. 92 (1–2) (2001) 17–34 (URL http://www.ncbi.nlm.nih.gov/pubmed/11527576).
[36] V.A. Selivanov, T.V. Votyakova, J.A. Zeak, M. Trucco, J. Roca, M. Cascante, Bistability of mitochondrial respiration underlies paradoxical reactive oxygen species generation induced by anoxia, PLoS Comput. Biol. 5 (12) (2009) e1000619, http://dx.doi.org/10.1371/journal.pcbi.1000619 (URL http://www.pubmedcentral.nih.gov/articlerender.fcgi?artid=2789320&tool=pmcentrez&rendertype=abstract).
[37] V.A. Selivanov, T.V. Votyakova, V.N. Pivtoraiko, J. Zeak, T. Sukhomlin, M. Trucco, J. Roca, M. Cascante, Reactive oxygen species production by forward and reverse electron fluxes in the mitochondrial respiratory chain, PLoS Comput. Biol. 7 (3) (2011) e1001115, http://dx.doi.org/10.1371/journal.pcbi.1001115 (URL http://www.ncbi.nlm.nih.gov/pubmed/21483483).
[38] O.V. Demin, B.N. Kholodenko, V.P. Skulachev, A model of $O_2^{\cdot-}$ generation in the complex III of the electron transport chain, Mol. Cell. Biochem. 184 (1–2) (1998) 21–33, http://dx.doi.org/10.1023/B:PRES.0000040434.77061.ca (URL http://www.ncbi.nlm.nih.gov/pubmed/9746310).
[39] C.L. Quinlan, A.A. Gerencser, J.R. Treberg, M.D. Brand, The mechanism of superoxide production by the antimycin-inhibited mitochondrial Q-cycle, J. Biol. Chem. 286 (2011) 31361–31372, http://dx.doi.org/10.1074/jbc.M111.267898 (URL http://www.ncbi.nlm.nih.gov/pubmed/21708945).
[40] J.N. Bazil, K.C. Vinnakota, F. Wu, D.A. Beard, Analysis of the kinetics and bistability of ubiquinol:cytochrome *c* oxidoreductase, Biophys. J. 105 (2) (2013) 343–355, http://dx.doi.org/10.1016/j.bpj.2013.05.033 (URL http://www.ncbi.nlm.nih.gov/pubmed/23870256).
[41] O. Demin, I. Goryanin, B. Kholodenko, H. Westerhoff, Kinetic modeling of energy metabolism and superoxide generation in hepatocyte mitochondria, Mol. Biol. 35 (6) (2001) 940–949 (URL http://www.springerlink.com/index/UP583278114040 77.pdf).
[42] J.W. Cooley, A structural model for across membrane coupling between the Q_o and Q_i active sites of cytochrome bc_1, Biochim. Biophys. Acta 1797 (12) (2010) 1842–1848, http://dx.doi.org/10.1016/j.bbabio.2010.05.013 (URL http://www.ncbi.nlm.nih.gov/pubmed/20513347).
[43] H. Baum, J.S. Rieske, H.I. Silman, S.H. Lipton, On the mechanism of electron transfer in complex III of the electron transfer chain, Proc. Natl. Acad. Sci. U. S. A. 57 (3) (1967) 798–805 (URL http://www.ncbi.nlm.nih.gov/pmc/articles/PMC335578/ http://www.ncbi.nlm.nih.gov/pubmed/335578 http://www.pubmedcentral.nih.gov/articlerender.fcgi?artid=335578&tool=pmcentrez&rendertype=abstract).
[44] U. Brandt, U. Haase, H. Schägger, G. von Jagow, Significance of the "Rieske" iron–sulfur protein for formation and function of the ubiquinol-oxidation pocket of mitochondrial cytochrome *c* reductase (bc_1 complex), J. Biol. Chem. 266 (30) (1991) 19958–19964 (URL http://www.ncbi.nlm.nih.gov/pubmed/1657909).
[45] J. Boork, The influence of membrane potentials on reaction rates. Control in free-energy-transducing systems, Biochim. Biophys. Acta Bioenerg. 767 (2) (1984) 314–320, http://dx.doi.org/10.1016/0005-2728(84)90201-9.
[46] J.A. Reynolds, E.A. Johnson, C. Tanford, Incorporation of membrane potential into theoretical analysis of electrogenic ion pumps, Proc. Natl. Acad. Sci. U. S. A. 82 (20) (1985) 6869–6873 (URL http://www.pubmedcentral.nih.gov/articlerender.fcgi?artid=390789&tool=pmcentrez&rendertype=abstract).
[47] C.C. Moser, J.L.R. Anderson, P.L. Dutton, Guidelines for tunneling in enzymes, Biochim. Biophys. Acta 1797 (9) (2010) 1573–1586, http://dx.doi.org/10.1016/j.bbabio.2010.04.441 (URL http://www.ncbi.nlm.nih.gov/pubmed/20460101).
[48] C.C. Moser, T.A. Farid, S.E. Chobot, P.L. Dutton, Electron tunneling chains of mitochondria, Biochim. Biophys. Acta 1757 (9–10) (2006) 1096–1109, http://dx.doi.org/10.1016/j.bbabio.2006.04.015 (URL http://www.ncbi.nlm.nih.gov/pubmed/16780790).
[49] S. Hoops, S. Sahle, R. Gauges, C. Lee, J. Pahle, N. Simus, M. Singhal, L. Xu, P. Mendes, U. Kummer, COPASI—a COmplex PAthway SImulator, Bioinformatics (Oxford, England) 22 (24) (2006) 3067–3074, http://dx.doi.org/10.1093/bioinformatics/btl485 (URL http://www.ncbi.nlm.nih.gov/pubmed/17032683).
[50] G. Benard, B. Faustin, E. Passerieux, A. Galinier, C. Rocher, N. Bellance, J.-P. Delage, L. Casteilla, T. Letellier, R. Rossignol, Physiological diversity of mitochondrial oxidative phosphorylation, Am. J. Physiol. Cell Physiol. 291 (6) (2006) C1172–C1182, http://dx.doi.org/10.1152/ajpcell.00195.2006 (URL http://www.ncbi.nlm.nih.gov/pubmed/16807301).
[51] S. Ransac, J.-P. Mazat, How does antimycin inhibit the bc_1 complex? A part-time twin, Biochim. Biophys. Acta 1797 (12) (2010) 1849–1857, http://dx.doi.org/10.1016/j.bbabio.2010.05.014 (URL http://www.ncbi.nlm.nih.gov/pubmed/20529661).
[52] S.M. Jin, M. Lazarou, C. Wang, L.A. Kane, D.P. Narendra, R.J. Youle, Mitochondrial membrane potential regulates PINK1 import and proteolytic destabilization by PARL, J. Cell Biol. 191 (5) (2010) 933–942, http://dx.doi.org/10.1083/jcb.201008084 (URL http://www.pubmedcentral.nih.gov/articlerender.fcgi?artid=2995166&tool=pmcentrez&rendertype=abstract).
[53] H. Rottenberg, R. Covian, B.L. Trumpower, Membrane potential greatly enhances superoxide generation by the cytochrome bc_1 complex reconstituted into phospholipid vesicles, J. Biol. Chem. 284 (29) (2009) 19203–19210, http://dx.doi.org/10.1074/jbc.M109.017376 (URL http://www.pubmedcentral.nih.gov/articlerender.fcgi?artid=2740544&tool=pmcentrez&rendertype=abstract).
[54] S. Ransac, N. Parisey, J.-P. Mazat, The loneliness of the electrons in the bc_1 complex, Biochim. Biophys. Acta 1777 (7–8) (2008) 1053–1059, http://dx.doi.org/10.1016/j.bbabio.2008.05.003 (URL http://www.ncbi.nlm.nih.gov/pubmed/18534187).
[55] J.L. Cape, M.K. Bowman, D.M. Kramer, A semiquinone intermediate generated at the Q_o site of the cytochrome bc_1 complex: importance for the Q-cycle and superoxide production, Proc. Natl. Acad. Sci. U. S. A. 104 (19) (2007) 7887–7892, http://dx.doi.org/10.1073/pnas.0702621104 (URL http://www.pubmedcentral.nih.gov/articlerender.fcgi?artid=1876542&tool=pmcentrez&rendertype=abstract).
[56] J. Zhu, T. Egawa, S.-r. Yeh, L. Yu, C.-a. Yu, Simultaneous reduction of iron–sulfur protein and cytochrome b_L during ubiquinol oxidation in cytochrome bc_1 complex, Proc. Natl. Acad. Sci. U. S. A. 104 (12) (2007) 4864–4869, http://dx.doi.org/10.1073/pnas.0607812104 (URL http://www.pubmedcentral.nih.gov/articlerender.fcgi?artid=1829230&tool=pmcentrez&rendertype=abstract).
[57] T.V. Votyakova, I.J. Reynolds, DeltaPsi(m)-dependent and -independent production of reactive oxygen species by rat brain mitochondria, J. Neurochem. 79 (2) (2001) 266–277, http://dx.doi.org/10.1046/j.1471-4159.2001.00548.x (URL http://doi.wiley.com/10.1046/j.1471-4159.2001.00548.x http://www.ncbi.nlm.nih.gov/pubmed/11677254).
[58] G. Twig, A. Elorza, A.J.A. Molina, H. Mohamed, J.D. Wikstrom, G. Walzer, L. Stiles, S.E. Haigh, S. Katz, G. Las, J. Alroy, M. Wu, B.F. Py, J. Yuan, J.T. Deeney, B.E. Corkey, O.S. Shirihai, Fission and selective fusion govern mitochondrial segregation and elimination by autophagy, EMBO J. 27 (2) (2008) 433–446, http://dx.doi.org/10.1038/sj.emboj.7601963 (URL http://www.pubmedcentral.nih.gov/articlerender.fcgi?artid=2234339&tool=pmcentrez&rendertype=abstract).
[59] E.L. Bell, T.A. Klimova, J. Eisenbart, C.T. Moraes, M.P. Murphy, G.R.S. Budinger, N.S. Chandel, The Q_o site of the mitochondrial complex III is required for the transduction of hypoxic signaling via reactive oxygen species production, J. Cell Biol. 177 (6) (2007) 1029–1036, http://dx.doi.org/10.1083/jcb.200609074 (URL http://www.pubmedcentral.nih.gov/articlerender.fcgi?artid=2064363&tool=pmcentrez&rendertype=abstract).
[60] H. Acker, The oxygen sensing signal cascade under the influence of reactive oxygen species, Philos. Trans. R. Soc. Lond. Ser. B Biol. Sci. 360 (1464) (2005) 2201–2210, http://dx.doi.org/10.1098/rstb.2005.1760 (URL http://www.pubmedcentral.nih.gov/articlerender.fcgi?artid=1569600&tool=pmcentrez&rendertype=abstract).
[61] R.B. Hamanaka, N.S. Chandel, Mitochondrial reactive oxygen species regulate cellular signaling and dictate biological outcomes, Trends Biochem. Sci. 35 (9) (2010) 505–513, http://dx.doi.org/10.1016/j.tibs.2010.04.002 (URL http://www.pubmedcentral.nih.gov/articlerender.fcgi?artid=2933303&tool=pmcentrez&rendertype=abstract).
[62] S. Dröse, P.J. Hanley, U. Brandt, Ambivalent effects of diazoxide on mitochondrial ROS production at respiratory chain complexes I and III, Biochim. Biophys. Acta 1790 (6) (2009) 558–565, http://dx.doi.org/10.1016/j.bbagen.2009.01.011 URL http://www.ncbi.nlm.nih.gov/pubmed/19364480 .